SSRG International Journal of Electrical and Electronics Engineering
ISSN: 2348-8379/ https://doi.org/10.14445/23488379/IJEEE-V12I10P115

Volume 12 Issue 10, 203-216, October 2025

Original Article

Robust Finite-Time Adaptive Flight Controller for Trajectory Tracking of a Quad-Rotor UAV Using a Recursive Sliding Mode Control Approach

Cristhian Mirko Ccorimanya Alvarez[1], Edson Dario Ccolla Pariapaza[2], Lizardo Pari[3]

[1,2,3]*Universidad Nacional de San Agustin de Arequipa, Arequipa, Peru.*

[1]*Corresponding Author : cccorimanya@unsa.edu.pe*

Received: 11 August 2025 Revised: 12 September 2025 Accepted: 15 October 2025 Published: 30 October 2025

Abstract - *This study addresses the trajectory tracking problem of an underactuated quad-rotor subjected to perturbations and uncertainties of modeling using a finite-time adaptive robust control approach. Considering the nonlinear, highly coupled, and underactuated nature of the 6DOF quad-rotor dynamics, the control system is decomposed into two subsystems: fully actuated and underactuated. A novel recursive sliding mode controller technique is developed for both subsystems, combining a PID-type sliding manifold with a fast terminal integral sliding manifold. Additionally, robust adaptive rules are developed to estimate the uncertain upper bound of exogenous perturbations. The proposed control approach ensures that the tracking errors of each subsystem stabilize at the origin within finite time and remain within a bounded neighborhood, even in the presence of large perturbations. A rigorous theoretical analysis based on Lyapunov theory is conducted to demonstrate the finite-time stability of each control subsystem. Finally, the performance of the developed control framework is validated through simulations in Matlab/Simulink, as well as through its implementation in ROS/Gazebo. A comparative analysis is also conducted against previously reported underactuated control strategies in the literature. Performance metrics such as RMSE and settling time are employed to verify the superiority of the developed method.*

Keywords - *SMC, Backstepping, Control systems, Quad-rotor, Trajectory tracking.*

1. Introduction

Quad-rotors are a type of UAV widely employed across various application domains, including industrial, civil, and military sectors [1]. Their popularity stems from numerous advantages, such as flight flexibility, compact size, and high maneuverability [2], making them particularly suitable for various tasks. However, despite these benefits, quad-rotors are classified as underactuated mechanical systems, possessing six-DOF but four control inputs [3]. This inherent limitation poses significant challenges for flight control, which are further exacerbated by the highly nonlinear and coupled dynamics of the system [4]. Due to these challenges, quad-rotor control has become a prominent and actively explored research topic within the fields of robotics and control. In particular, the problem of trajectory tracking has attracted significant interest in the existing literature. Various linear control strategies have been applied to this task, including PID [5], LQR [6], state feedback control [7], and Model Predictive Control (MPC) [8]. However, as quad-rotors are underactuated systems with strongly nonlinear dynamics, linear methods, based on system linearization around an equilibrium point, often fail to maintain satisfactory performance under significant variations in operating conditions [9]. In particular, in the presence of perturbations and uncertainties, linear controllers exhibit limited robustness and tracking accuracy. These limitations have been confirmed by experimental studies such as [10], where the effectiveness of a linear technique was compared to that of a nonlinear one for a robotic trajectory tracking task. In response to such limitations, various nonlinear type control strategies have been introduced in previous studies. Among the most prominent is Sliding Mode Control (SMC), renowned for its strong robustness against nonlinearities [11]. Moreover, advanced sliding surfaces allow fast convergence toward the reference trajectory [12]. Owing to these characteristics, SMC has become a prevalent strategy for controlling different mechanical systems with nonlinear behavior, including robotic manipulators [13], underwater vehicles [14], ground mobile robots [15], and UAV quad-rotors [16]. In the context of quad-rotor control, several SMC approaches have been proposed. For instance, in [17], the authors developed a robust control strategy founded on recursive SMC, augmented with adaptive laws to alleviate the effects of perturbations. In [18], an integral SMC approach was introduced, combined with an observer, to reject perturbations and enhance system robustness. However, both works [17, 18] focus only on the

attitude dynamics for trajectory tracking without considering the full dynamics (i.e., both attitude and position), which limits their practical applicability in scenarios where complete motion control is essential. Conversely, some studies have tackled the trajectory tracking challenge considering the full dynamics of the quad-rotor. In [19], an adaptive control technique based on an integral terminal SMC was suggested to regulate both the position and attitude of the quad-rotor. In [20], the researchers presented a finite-time hybrid control scheme combining an integral SMC for altitude, a backstepping controller for horizontal position, and a nonsingular terminal SMC for attitude, with an embedded disturbance observer to enhance robustness.

Similarly, in [21], a fast-converging finite-time control law based on a global fractional-order SMC was introduced for the full quad-rotor UAV dynamics. While these works [19-21] consider the complete system dynamics and apply advanced sliding mode techniques, it is worth noting that they all adopt a control structure involving three virtual control inputs for position dynamics and three physical control inputs for attitude dynamics, thus resulting in a fully actuated system. This formulation does not reflect the underactuated nature of a quad-rotor, which inherently has six-DOF while being driven by only four control inputs.

An alternative line of research has proposed SMC-based strategies that explicitly respect the underactuated structure of the system. These strategies commonly partition the control design into two parts: the fully actuated and the underactuated subsystems [22]. One of the early works adopting this methodology is [23], where a second-order SMC was developed for tracking both position and attitude. This was later extended in [24] with an adaptive control scheme relying on neural networks to compensate for disturbances and uncertainties.

More recently, in [25], an enhanced dual SMC approach based on a U-model was proposed, incorporating an extended state observer for disturbance estimation. While these studies [23-25] address the underactuated nature of the system-using only the four physical inputs to regulate all six degrees of freedom-they rely on conventional linear sliding manifolds, which merely guarantee asymptotic convergence of the tracking error [12]. Consequently, the convergence rate cannot be explicitly bounded in finite time, which poses a significant limitation for practical applications requiring rapid responses, such as formation control in multi-quadrotor systems [26].

Motivated by these limitations, this study proposes a novel finite-time robust flight control scheme based on a recursive SMC architecture that incorporates nonlinear sliding manifolds to provide rapid convergence and accurate path tracking. The developed approach seeks to handle the trajectory tracking task for the full dynamics of an underactuated quad-rotor under significant perturbations and uncertainties. The flight control framework respects the underactuated nature of the system-namely, only four control laws are designed for a six-DOF system-and aims to enhance robustness and convergence speed performance.

The findings and contributions of the present research are highlighted below:

- Different from the frameworks proposed in [23-25], which employ conventional linear sliding surfaces, this work proposes an innovative adaptive recursive sliding mode control scheme that integrates a PID-based sliding manifold with a fast terminal integral sliding manifold. This combination enables reliable and effective control for trajectory tracking in underactuated quad-rotor systems.
- The developed control strategy ensures global stability within a finite time by driving the tracking errors to vanish rapidly. In addition, the adaptive mechanisms incorporated are capable of compensating for strong perturbations, which in turn strengthen the robustness of the system.
- The study is validated through implementation in two simulation environments: Matlab/Simulink and the ROS/Gazebo operating system. Additionally, a comparison was carried out against the control schemes presented in [24, 25, 27], demonstrating the enhanced robustness and faster convergence of the proposed method.

The subsequent sections of this research are arranged as follows: Section 2 outlines the mathematical model of the quad-rotor and defines the control objectives. Section 3 details the formulation of the proposed control scheme. Section 4 analyzes the results of the simulations, and Section 5 highlights the main conclusions.

2. Mathematical Model and Problem Formulation

In this study, the Parrot Mambo quad-rotor is adopted as the reference model [28]. This type of aerial platform is classified as a mechanically underactuated system, as it has six DOF-three associated with position (x, y, z), and three with orientation (ϕ, θ, ψ), corresponding to the Euler angles roll, pitch, and yaw, respectively. However, the system offers just four action inputs: one corresponding to the vertical thrust and three associated with the torques about the pitch, roll, and yaw axes [2, 3].

The four-rotor robot motion in space is described using two reference frames (see Figure 1): the inertial frame $E = \left(E_x, E_y, E_z\right)$ for translational dynamics in Cartesian space (x, y, z); and the body-attached frame $B = \left(B_x, B_y, B_z\right)$ is introduced to capture the rotational dynamics using the Euler angle representation.

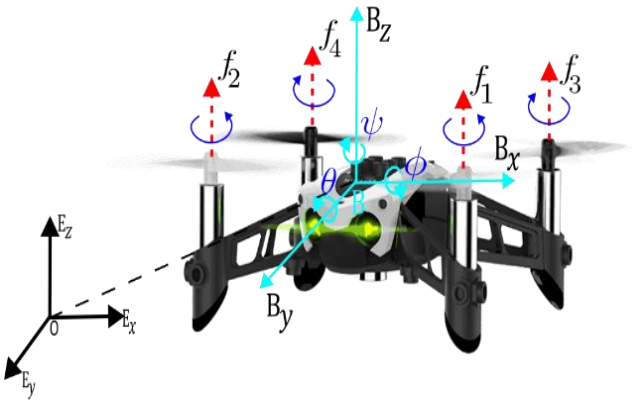

Fig. 1 Parrot Mambo quad-rotor aircraft

2.1. Dynamic Model of the Quad-Rotor UAV

Several previous studies have investigated the mathematical modeling of quad-rotors using Newton-Euler and Euler-Lagrange approaches [1]. The positional and attitudinal behavior of the four-rotor aerial robot can be modeled [2]:

$$\begin{aligned}
\ddot{x} &= \frac{1}{m_q}[(c\phi\, s\theta\, c\psi + s\phi\, s\psi)u_1 - k_x\dot{x}] + D_x(t),\\
\ddot{y} &= \frac{1}{m_q}\left[(c\phi s\theta s\psi - s\phi c\psi)u_1 - k_y\dot{y}\right] + D_y(t),\\
\ddot{z} &= \frac{1}{m_q}[(c\phi c\theta)u_1 - k_z\dot{z}] - g + D_z(t),\\
\ddot{\phi} &= \frac{1}{J_x}\Big[(J_y - J_z)\dot{\theta}\dot{\psi} - J_r\dot{\theta}\underline{\omega} - k_\phi\dot{\phi}^2 + u_2 + D_\phi(t)\Big],\\
\ddot{\theta} &= \frac{1}{J_y}\Big[(J_z - J_x)\dot{\phi}\dot{\psi} + J_r\dot{\phi}\underline{\omega} - k_\theta\dot{\theta}^2 + u_3 + D_\theta(t)\Big],\\
\ddot{\psi} &= \frac{1}{J_z}\Big[(J_x - J_y)\dot{\phi}\dot{\theta} - k_\psi\dot{\psi}^2 + u_4 + D_\psi(t)\Big],
\end{aligned} \tag{1}$$

Where c(·) = cos(·), s(·) = sin(·), $\underline{\omega} = \Omega_1 - \Omega_2 + \Omega_3 - \Omega_4$ specifies the aircraft's angular velocity, u_1 indicating the total thrust force, and u_2, u_3, u_4 correspond to torques in the roll, pitch, and yaw axes. These four terms constitute the actuation inputs of the underactuated dynamics. The functions $D_x(t), D_y(t), D_z(t), D_\phi(t), D_\theta(t)$, and $D_\psi(t)$ denote external perturbations that vary over time. This study employs the Parrot Mambo quad-rotor as the reference model [28]. The physical parameters of the quad-rotor are: mass $m_q(kg)$, gravitational constant $g(m/s^2)$, inertia components $J_x, J_y, J_z(kg \cdot m^2)$, drag coefficients $k_x, k_y, k_z(N \cdot s/m)$, friction coefficients $k_\phi, k_\theta, k_\psi(N \cdot s/rad)$, and rotor inertia $J_r(kg \cdot m^2)$. The actuator-generated control signals u_1, u_2, u_3, and u_4 are calculated as functions of the rotational velocities of the quad-rotor's four propellers, as expressed below [9]:

$$\begin{bmatrix} u_1 \\ u_2 \\ u_3 \\ u_4 \end{bmatrix} = \begin{bmatrix} G_t & G_t & G_t & G_t \\ -G_t l & G_t l & G_t l & -G_t l \\ Gl & -G_t l & G_t l & -G_t l \\ -G_d & -G_d & G_d & G_d \end{bmatrix} \begin{bmatrix} \Omega_1 \\ \Omega_2 \\ \Omega_3 \\ \Omega_4 \end{bmatrix}, \tag{2}$$

Where G_t stands for the thrust coefficient, G_d designates the drag coefficient, and l indicates the distance from the rotors and the body's center of mass.

2.2. Problem Formulation

To design an appropriate control system, the dynamics of the four-rotor aerial robot presented in Equation (1) can be reformulated into a first-order state-space representation as follows:

$$\dot{\chi} = f(\chi) + g(\chi)U + D, \tag{3}$$

Where $\chi = \left[\, x, \dot{x},\, y, \dot{y},\, z, \dot{z},\, \phi, \dot{\phi},\, \theta, \dot{\theta},\, \psi, \dot{\psi} \,\right]^T \in R^{12}$ denotes the state vector. The terms $f(\chi) \neq 0$ and $g(\chi) \neq 0$ are nonlinear mappings, while $U = [u_1, u_2, u_3, u_4]^T \in R^4$ represents the control input vector of the dynamic system. Finally, $D = \left[D_x, D_y, D_z, D_\phi, D_\theta, D_\psi\right]^T \in R^6$ corresponds to the external time-varying perturbations. From the preceding formulation, the system can be formulated in the following manner:

$$\begin{cases}
\dot{\chi}_1 = \chi_2, \\
\dot{\chi}_2 = f_x + g_x u_1 + D_x, \\
\dot{\chi}_3 = \chi_4, \\
\dot{\chi}_4 = f_y + g_y u_1 + D_y, \\
\dot{\chi}_5 = \chi_6, \\
\dot{\chi}_6 = f_z + g_z u_1 + D_z, \\
\dot{\chi}_7 = \chi_8, \\
\dot{\chi}_8 = f_\phi + g_\phi u_2 + D_\phi, \\
\dot{\chi}_9 = \chi_{10}, \\
\dot{\chi}_{10} = f_\theta + g_\theta u_3 + D_\theta, \\
\dot{\chi}_{11} = \chi_{12}, \\
\dot{\chi}_{12} = f_\psi + g_\psi u_4 + D_\psi,
\end{cases} \tag{4}$$

Where the nonlinear functions are described as follows:

$$
\begin{aligned}
&f_x = -k_x\dot{x}, f_y = -k_y\dot{y}, f_z = -k_z\dot{z} - g,\\
&f_\phi = \frac{1}{J_x}\left[(J_y - J_z)\dot{\theta}\dot{\psi} - J_r\dot{\theta}\underline{\omega} - k_\phi\dot{\phi}^2\right],\\
&f_\theta = \frac{1}{J_y}\left[(J_z - J_x)\dot{\phi}\dot{\psi} + J_r\dot{\phi}\underline{\omega} - k_\theta\dot{\theta}^2\right],\\
&f_\psi = \frac{1}{J_z}\left[(J_x - J_y)\dot{\phi}\dot{\theta} - k_\psi\dot{\psi}^2\right],\\
&g_x = \frac{1}{m_q}(c\phi\, s\theta\, c\psi + s\phi\, s\psi),\\
&g_y = \frac{1}{m_q}(c\phi s\theta s\psi - s\phi c\psi), g_z = \frac{1}{m_q}(c\phi c\theta),\\
&g_\phi = \frac{1}{J_x}, g_\theta = \frac{1}{J_y}, g_\psi = \frac{1}{J_z}.
\end{aligned}
\tag{5}
$$

Remark 1. The formulation of the quad-rotor's dynamics given in Equation (4) corresponds to a multi-input, multi-output, nonlinear, coupled, and underactuated system, which is also subject to time-varying external disturbances. These characteristics make the control design particularly challenging.

Consequently, it becomes essential to design a strong and trustworthy flight controller that can successfully deal with these difficulties.

According to Remark 1, the quad-rotor robot is considered an under-actuated system. This challenge can be addressed by decomposing the system structure into two subsystems, following approaches inspired by the works in [23, 24].

The first subsystem is fully actuated and controlled by the inputs u_1 and u_4, which regulate the states (z, ψ). The second subsystem is underactuated and utilizes u_2 and u_3 to control the coupled states (x, ϕ) and (y, θ), respectively. These subsystems are defined as follows:

$$
\begin{aligned}
&fully\ actuated \begin{cases} \dot{\chi_5} = \chi_6 \\ \dot{\chi_6} = f_z + g_z u_1 \\ \dot{\chi_{11}} = \chi_{12} \\ \dot{\chi_{12}} = f_\psi + g_\psi u_4 \end{cases},\\
&under\ actuated \begin{cases} \dot{\chi_1} = \chi_2 \\ \dot{\chi_2} = f_x + g_x u_1 \\ \dot{\chi_3} = \chi_4 \\ \dot{\chi_4} = f_y + g_y u_1 \\ \dot{\chi_7} = \chi_8 \\ \dot{\chi_8} = f_\phi + g_\phi u_2 \\ \dot{\chi_9} = \chi_{10} \\ \dot{\chi_{10}} = f_\theta + g_\theta u_3 \end{cases}
\end{aligned}
\tag{6}
$$

Based on this decomposition, the scope of this investigation is to elaborate a robust and efficient flight scheme for a nonlinear, coupled, and under-actuated system like the quad-rotor UAV. The proposed framework is required to meet the following conditions:

- The flight control system must be robust and capable of adapting to dynamic changes in the environment and in the model.
- The trajectory tracking errors are required to reach the origin in a finite time and remain within its neighborhood even under perturbations.
- The generated control signals should be singularity-free and avoid chattering effects.

3. Flight Control System Design

On the basis of the problem formulation described earlier, this section describes the control framework designed. The control architecture is organized into two components: a fully actuated part and an underactuated one. For both cases, a novel finite-time adaptive recursive sliding mode controller is introduced in the present research to tackle the trajectory tracking challenge of a four-rotor UAV nonlinear and underactuated system. The schematic representation of the proposed methodology is depicted in Figure 2.

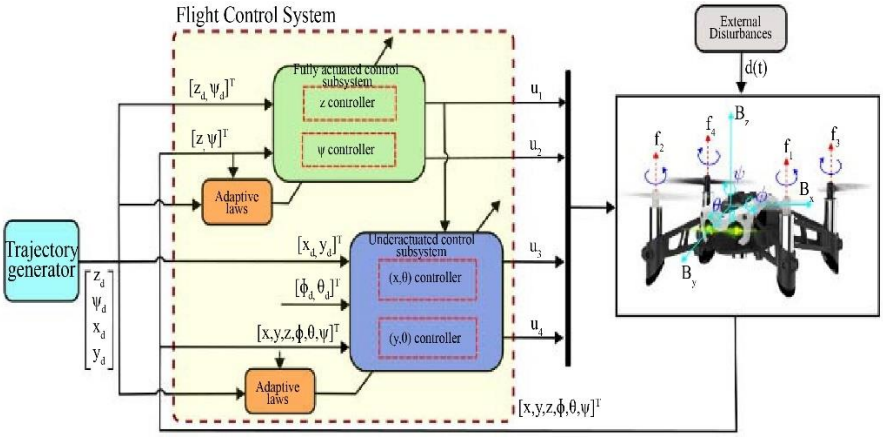

Fig. 2 The diagram of the suggested control scheme

3.1. Fully Actuated Control Subsystem

The quad-rotor's fully actuated control subsystem consists of the input vector $[u_1,\ u_4]^T$and the output vector $[z, \psi]^T$.

For this subsystem, the tracking errors are defined as:

$$\begin{bmatrix} e_z \\ e_\psi \end{bmatrix} = \begin{bmatrix} z_d - z \\ \psi_d - \psi \end{bmatrix}, \quad \begin{bmatrix} \dot{e_z} \\ \dot{e_\psi} \end{bmatrix} = \begin{bmatrix} \dot{z_d} - \dot{z} \\ \dot{\psi_d} - \dot{\psi} \end{bmatrix}. \tag{7}$$

Based on the works in [23, 24], the fully actuated subsystem is designed with the following PID-based sliding manifolds:

$$\begin{bmatrix} \sigma_z \\ \sigma_\psi \end{bmatrix} = \begin{bmatrix} k_{p_z}\, e_z \ + \ k_{i_z} \int e_z \ dt \ + \ k_{d_z}\, \dot{e}_z \\ k_{p_\psi}\, e_\psi \ + \ k_{i_\psi} \int e_\psi \ dt \ + \ k_{d_\psi}\, \dot{e}_\psi \end{bmatrix}, \tag{8}$$

where k_{p_j}, k_{i_j}, and k_{d_j} for $j = \{z, \psi\}$ are strictly positive controller gains. The time derivative of Equation (8) is given by:

$$\begin{bmatrix} \dot{\sigma}_z \\ \dot{\sigma}_\psi \end{bmatrix} = \begin{bmatrix} k_{p_z}\, \dot{e}_z \ + \ k_{i_z} e_z \ + \ k_{d_z} \ddot{e}_z \\ k_{p_\psi}\, \dot{e}_\psi \ + \ k_{i_\psi} e_\psi \ + \ k_{d_\psi} \ddot{e}_\psi \end{bmatrix} \tag{9}$$

To achieve fast convergence of the fully actuated subsystem states, a new recursive integral sliding surface is proposed, defined as:

$$\begin{bmatrix} s_z \\ s_\psi \end{bmatrix} = \begin{bmatrix} \sigma_z \ + \ \beta_z \int \left(|\sigma_z|^{\lambda_z} \operatorname{sgn}(\sigma_z) \ + \ \alpha_z\, \sigma_z \right) dt \\ \sigma_\psi \ + \ \beta_\psi \int \left(|\sigma_\psi|^{\lambda_\psi} \operatorname{sgn}(\sigma_\psi) \ + \ \alpha_\psi\, \sigma_\psi \right) dt \end{bmatrix} \tag{10}$$

where α_j, β_j for $j = \{z, \psi\}$ are positive constants representing the control gains. The exponents λ_j satisfy $0 < \lambda_j < 1$.

The time derivative of Equation (10) is expressed as:

$$\begin{bmatrix} \dot{s}_z \\ \dot{s}_\psi \end{bmatrix} = \begin{bmatrix} \dot{\sigma}_z \ + \ \beta_z \left(|\sigma_z|^{\lambda_z} \operatorname{sgn}(\sigma_z) \ + \ \alpha_z\, \sigma_z \right) \\ \dot{\sigma}_\psi \ + \ \beta_\psi \left(|\sigma_\psi|^{\lambda_\psi} \operatorname{sgn}(\sigma_\psi) \ + \ \alpha_\psi\, \sigma_\psi \right) \end{bmatrix} \tag{11}$$

By enforcing the sliding mode control condition, i.e., $\dot{s}_z \ = \dot{s}_\psi \ = 0$ [29, 30], the equivalent control laws for the fully actuated subsystem are derived as indicated below:

$$\begin{aligned} u_{eq}^z &= \tfrac{1}{k_{d_z} g_z} \left[k_{p_z} \dot{e_z} + k_{i_z} e_z + k_{d_z} \ddot{z_d} - k_{d_z} f_z + \right. \\ &\quad \left. \beta_z \left(|\sigma_z|^{\lambda_z} \operatorname{sgn}(\sigma_z) + \alpha_z \sigma_z \right) \right], \\ u_{eq}^\psi &= \tfrac{1}{k_{d_\psi} g_\psi} \left[k_{p_\psi} \dot{e_\psi} + k_{i_\psi} e_\psi + k_{d_\psi} \ddot{\psi}_d - \right. \\ &\quad \left. k_{d_\psi} f_\psi + \beta_\psi \left(|\sigma_\psi|^{\lambda_\psi} \operatorname{sgn}(\sigma_\psi) + \alpha_\psi \sigma_\psi \right) \right]. \end{aligned} \tag{12}$$

To attain rapid finite-time convergence of the system trajectories to the sliding manifolds, the reaching control schemes described below are formulated:

$$\begin{aligned} u_r^z &= \tfrac{1}{k_{d_z} g_z} \left[\hat{K}_1^z \operatorname{sgn}^{\eta_{1,z}}(s_z) + \hat{K}_2^z \operatorname{sgn}^{\eta_{2,z}}(s_z) \right], \\ u_r^\psi &= \tfrac{1}{k_{d_\psi} g_\psi} \left[\hat{K}_1^\psi \operatorname{sgn}^{\eta_{1,\psi}}(s_\psi) + \hat{K}_2^\psi \operatorname{sgn}^{\eta_{2,\psi}}(s_\psi) \right], \end{aligned} \tag{13}$$

Where the exponents $\eta_{1,j}, \eta_{2,j}$ for $j = \{z, \psi\}$ satisfy the inequality $0 < \eta_{m,i} < 1$ for $m = \{1,2\}$.The expressions $\hat{K}_1^z, \hat{K}_2^z, \hat{K}_1^\psi, \hat{K}_2^\psi$ are the adaptive estimates of the unknown bounds $K_1^z, K_2^z, K_1^\psi, K_2^\psi$, and are updated according to the adaptation signals below:

$$\begin{cases} \dot{\hat{K}}_1^z = \mu_1^z |s_z|^{\eta_{1,z}+1} \\ \dot{\hat{K}}_2^z = \mu_2^z |s_z|^{\eta_{2,z}+1} \\ \dot{\hat{K}}_1^\psi = \mu_1^\psi |s_\psi|^{\eta_{1,\psi}+1} \\ \dot{\hat{K}}_2^\psi = \mu_2^\psi |s_\psi|^{\eta_{2,\psi}+1} \end{cases} \tag{14}$$

Finally, by summing the expressions corresponding to the equivalent control laws in Equation (12) and the reaching control laws in Equation (13), the final control inputs for the fully actuated are obtained as:

$$\begin{bmatrix} u_1 \\ u_4 \end{bmatrix} = \begin{bmatrix} u_{eq}^z + u_r^z \\ u_{eq}^\psi + u_r^\psi \end{bmatrix} \tag{15}$$

Theorem 1: Consider the fully actuated subsystem defined in Equation (6), together with the control laws designed in Equation (15) and the adaptation laws presented in Equation (14). Under these conditions, the errors of the subsystem, as set out in Equation (7), are guaranteed to converge to the origin in finite time and remain within a neighborhood of it.

Proof. 1: To settle Theorem 1, the Lyapunov theory is applied using the direct method. Hence, the following candidate Lyapunov function is proposed:

$$V_z = \tfrac{1}{2} s_z^2 + \tfrac{1}{2\mu_1^z} \left(\tilde{K}_1^z \right)^2 + \tfrac{1}{2\mu_2^z} \left(\tilde{K}_2^z \right)^2 \tag{16}$$

Where $\tilde{K}_1^z = \hat{K}_1^z - K_1^z$ and $\tilde{K}_2^z = \hat{K}_2^z - K_2^z$ denote the estimation errors associated with the adaptive laws. By computing the time derivative of the chosen Lyapunov function, one obtains:

$$\begin{aligned} \dot{V}_z \ &= \ s_z\, \dot{s}_z \ + \ \tfrac{1}{\mu_1^z}\, \tilde{K}_1^z \dot{\tilde{K}}_1^z \ + \ \tfrac{1}{\mu_2^z}\, \tilde{K}_2^z\, \dot{\tilde{K}}_2^z \\ &= s_z \left[\dot{\sigma}_z + \beta_z \left(|\sigma_z|^{\lambda_z} \operatorname{sgn}(\sigma_z) + \alpha_z \sigma_z \right) \right] + \\ &\quad \tfrac{1}{\mu_1^z}\, \tilde{K}_1^z \dot{\tilde{K}}_1^z \ + \ \tfrac{1}{\mu_2^z}\, \tilde{K}_2^z\, \dot{\tilde{K}}_2^z \\ &= s_z \left[k_{p_z} \dot{e_z} + k_{i_z} e_z + k_{d_z} \ddot{e_z} + \right. \end{aligned}$$

$$\begin{aligned}
&\beta_z\left(|\sigma_z|^{\lambda_z}\text{sgn}(\sigma_z)+\alpha_z\sigma_z\right)\Big]+\tfrac{1}{\mu_1^z}\,\widetilde{K}_1^z\dot{\widetilde{K}}_1^z\;+\\
&\tfrac{1}{\mu_2^z}\,\widetilde{K}_2^z\,\dot{\widetilde{K}}_2^z\\
&=s_z\Big[k_{p_z}\dot{e}_z+k_{i_z}e_z+k_{d_z}\ddot{e}_z+\\
&\quad\beta_z\left(|\sigma_z|^{\lambda_z}\text{sgn}(\sigma_z)+\alpha_z\sigma_z\right)\Big]+\tfrac{1}{\mu_1^z}\,\widetilde{K}_1^z\dot{\widetilde{K}}_1^z\;+\\
&\quad\tfrac{1}{\mu_2^z}\,\widetilde{K}_2^z\,\dot{\widetilde{K}}_2^z\\
&=s_z\Big[k_{p_z}\dot{e}_z+k_{i_z}e_z+k_{d_z}(\ddot{z}_d-f_z-g_zu_1)+\\
&\quad\beta_z\left(|\sigma_z|^{\lambda_z}sgn(\sigma_z)+\alpha_z\sigma_z\right)\Big]+\tfrac{1}{\mu_1^z}\,\widetilde{K}_1^z\dot{\widetilde{K}}_1^z\;+\\
&\quad\tfrac{1}{\mu_2^z}\,\widetilde{K}_2^z\,\dot{\widetilde{K}}_2^z.
\end{aligned}\tag{17}$$

Substituting the control law u_1 into Equation (17) and performing the corresponding algebraic manipulations, we obtain:

$$\begin{aligned}
\dot{V}_z\;&=\;s_z\left[-\widehat{K}_1^z\text{sgn}^{n_{1,z}}(s_z)-\widehat{K}_2^z\text{sgn}^{n_{2,z}}(s_z)\right]+\\
&\quad\tfrac{\widetilde{K}_1^z}{\mu_1^z}\,(\mu_1^z\,|s_z|)^{n_{1,z}+1}+\tfrac{\widetilde{K}_2^z}{\mu_2^z}\,(\mu_2^z\,|s_z|)^{n_{2,z}+1}\\
&=-\widehat{K}_1^z|s_z|^{n_{1,z}+1}-\widehat{K}_2^z|s_z|^{n_{2,z}+1}+\\
&\quad K_1^z|s_z|^{n_{1,z}+1}+K_2^z|s_z|^{n_{2,z}+1}+K_1^z|s_z|^{n_{1,z}+1}-\\
&\quad K_1^z|s_z|^{n_{1,z}+1}+|s_z|^{n_{2,z}+1}-K_2^z|s_z|^{n_{2,z}+1}\\
&=-\widetilde{K}_1^z|s_z|^{n_{1,z}+1}-\widetilde{K}_2^z|s_z|^{n_{2,z}+1}+\\
&\quad\widetilde{K}_1^z|s_z|^{n_{1,z}+1}+\widetilde{K}_2^z|s_z|^{n_{2,z}+1}-K_1^z|s_z|^{n_{1,z}+1}-\\
&\quad K_2^z|s_z|^{n_{2,z}+1}\\
\dot{V}_z\;&\leq\;-K_1^z|s_z|^{n_{1,z}+1}-K_2^z|s_z|^{n_{2,z}+1}.
\end{aligned}\tag{18}$$

After performing some mathematical simplifications, the following expression is derived:

$$\begin{aligned}
\dot{V}_z\;&\leq\;-K_1^z\left|\tfrac{2s_z^2}{2}\right|^{\frac{n_{1,z}+1}{2}}-K_2^z\left|\tfrac{2s_z^2}{2}\right|^{\frac{n_{2,z}+1}{2}}.\\
\dot{V}_z\;&\leq\;-2K_1^z|V_z|^{\frac{n_{1,z}+1}{2}}-2K_2^z|V_z|^{\frac{n_{2,z}+1}{2}}.
\end{aligned}\tag{19}$$

According to Lemma 2 in reference [9], the tracking error e_z converges to the origin in finite time T_{f_1}, given by:

$$T_{f_1}=\frac{1}{2K_1^z(n_{1,z}-1)}+\frac{1}{2K_2^z(1-n_{2,z})}\tag{20}$$

Following the procedure applied in Proof 1, one can also verify that the error e_ψ vanishes in finite time T_{f_4}.

3.2. Under-Actuated Control Subsystem

The underactuated control subsystem of the quad-rotor consists of the inputs $[u_2,u_3]^T$ and the outputs $[x,y,\phi,\theta]^T$. The tracking errors for this subsystem are defined as:

$$\begin{bmatrix}e_x\\e_y\\e_\phi\\e_\theta\end{bmatrix}=\begin{bmatrix}x_d-x\\y_d-y\\\phi_d-\phi\\\theta_d-\theta\end{bmatrix},\quad\begin{bmatrix}\dot{e}_x\\\dot{e}_y\\\dot{e}_\phi\\\dot{e}_\theta\end{bmatrix}=\begin{bmatrix}\dot{x}_d-\dot{x}\\\dot{y}_d-\dot{y}\\\dot{\phi}_d-\dot{\phi}\\\dot{\theta}_d-\dot{\theta}\end{bmatrix}\tag{21}$$

For the underactuated control subsystem, the following PID-type sliding surfaces are proposed:

$$\begin{bmatrix}\sigma_\phi\\\sigma_\theta\end{bmatrix}=\begin{bmatrix}k_{p_\phi}e_\phi+k_{i_\phi}\int e_\phi\,dt+k_{d_\phi}\dot{e}_\phi+\\k_{p_y}e_y+k_{i_y}\int e_y\;dt+k_{d_y}\dot{e}_y\\k_{p_\theta}e_\theta+k_{i_\theta}\int e_\theta\,dt+k_{d_\theta}\dot{e}_\theta+\\k_{p_x}e_x+k_{i_x}\int e_x\;dt+k_{d_x}\dot{e}_x\end{bmatrix}\tag{22}$$

Where k_{p_i},k_{i_i}, and k_{d_i} with $i=\{x,y,\phi,\theta\}$ are positive nonzero constants. These coefficients are selected using Hurwitz stability analysis [23, 27].

Taking the time derivative of the surfaces in Equation (22), one obtains:

$$\begin{bmatrix}\dot{\sigma}_\phi\\\dot{\sigma}_\theta\end{bmatrix}=\begin{bmatrix}k_{p_\phi}\dot{e}_\phi+k_{i_\phi}e_\phi+k_{d_\phi}\ddot{e}_\phi+\\k_{p_y}\dot{e}_y+k_{i_y}e_y+k_{d_y}\ddot{e}_y\\k_{p_\theta}\dot{e}_\theta+k_{i_\theta}e_\theta+k_{d_\theta}\ddot{e}_\theta+\\k_{p_x}\dot{e}_x+k_{i_x}e_x+k_{d_x}\ddot{e}_x\end{bmatrix}\tag{23}$$

To achieve fast convergence of the states in the underactuated subsystem, a new recursive integral sliding surface is proposed, defined as:

$$\begin{bmatrix}s_\phi\\s_\theta\end{bmatrix}=\begin{bmatrix}\sigma_\phi+\beta_\phi\int\left(|\sigma_\phi|^{\lambda_\phi}\,\text{sgn}(\sigma_\phi)+\alpha_\phi\,\sigma_\phi\right)dt\\\sigma_\theta+\beta_\theta\int\left(|\sigma_\theta|^{\lambda_\theta}\,\text{sgn}(\sigma_\theta)+\,\alpha_\theta\,\sigma_\theta\right)dt\end{bmatrix}\tag{24}$$

Where α_i and β_i with $i=\{\phi,\theta\}$ are positive constants representing the control gains. The exponents λ_i for $i=\{\phi,\theta\}$ satisfy the inequality $0<\lambda_i<1$.

The time derivative of Equation (24) is given by:

$$\begin{bmatrix}\dot{s}_\phi\\\dot{s}_\theta\end{bmatrix}=\begin{bmatrix}\dot{\sigma}_\phi+\beta_\phi\left(|\sigma_\phi|^{\lambda_\phi}\,\text{sgn}(\sigma_\phi)+\alpha_\phi\,\sigma_\phi\right)\\\dot{\sigma}_\theta+\beta_\theta\left(|\sigma_\theta|^{\lambda_\theta}\,\text{sgn}(\sigma_\theta)+\alpha_\theta\,\sigma_\theta\right)\end{bmatrix}\tag{25}$$

By establishing the sliding mode control condition, i.e., $\dot{s_\phi}=\dot{s_\theta}=0$, the equivalent control laws for the underactuated subsystem are obtained as follows:

$$\begin{aligned}
u_{eq}^{\phi}=\frac{1}{k_{d_\phi}g_\phi}\Big[&k_{p_\phi}\dot{e_\phi}+k_{i_\phi}e_\phi+k_{d_\phi}\ddot{\phi_d}-k_{d_\phi}f_\phi\\
&+k_{p_y}\dot{e_y}+k_{i_y}e_y\\
&+k_{d_y}(\ddot{y_d}-\ddot{y})\,\beta_\phi\left(|\sigma_\phi|^{\lambda_\phi}\text{sgn}(\sigma_\phi)\right.\\
&\left.+\alpha_\phi\sigma_\phi\right)\Big]\\
u_{eq}^{\theta}=\frac{1}{k_{d_\theta}g_\theta}\Big[&k_{p_\theta}\dot{e_\theta}+k_{i_\theta}e_\theta+k_{d_\theta}\ddot{\theta_d}-k_{d_\theta}f_\theta\\
&+\;k_{p_x}\dot{e_x}+k_{i_x}e_x\\
&+k_{d_x}(\ddot{x_d}-\ddot{x})\,\beta_\theta\left(|\sigma_\theta|^{\lambda_\theta}\text{sgn}(\sigma_\theta)\right.\\
&\left.+\alpha_\theta\sigma_\theta\right)\Big]
\end{aligned}\tag{26}$$

In an attempt to achieve swift finite-time convergence of the system trajectories to the sliding manifolds, the reaching control laws defined below are presented:

$$\begin{aligned} u_r^{\phi} &= \frac{1}{k_{d_\phi} g_\phi}\left[\hat{K}_1^{\phi} sgn^{\eta_{1,\phi}}(s_\phi) + \hat{K}_2^{\phi} sgn^{\eta_{2,\phi}}(s_\phi)\right], \\ u_r^{\theta} &= \frac{1}{k_{d_\theta} g_\theta}\left[\hat{K}_1^{\theta} sgn^{\eta_{1,\theta}}(s_\theta) + \hat{K}_2^{\theta} sgn^{\eta_{2,\theta}}(s_\theta)\right], \end{aligned} \tag{27}$$

Where the exponents $\eta_{1,i}, \eta_{2,i}$ with $i = \{\phi, \theta\}$ satisfy the inequality $0 < \eta_{j,i} < 1$ for $j = 1, 2$, and the terms $\hat{K}_1^{\phi}, \hat{K}_2^{\phi}, \hat{K}_1^{\theta}, \hat{K}_2^{\theta}$ represent the adaptive estimates of $K_1^{\phi}, K_2^{\phi}, K_1^{\theta}, K_2^{\theta}$, determined by the following adaptive laws:

$$\begin{cases} \dot{\hat{K}}_1^{\phi} = \mu_1^{\phi} |s_\phi|^{\eta_{1,\phi}+1} \\ \dot{\hat{K}}_2^{\phi} = \mu_2^{\phi} |s_\phi|^{\eta_{2,\phi}+1} \\ \dot{\hat{K}}_1^{\theta} = \mu_1^{\theta} |s_\theta|^{\eta_{1,\theta}+1} \\ \dot{\hat{K}}_2^{\theta} = \mu_2^{\theta} |s_\theta|^{\eta_{2,\theta}+1} \end{cases} \tag{28}$$

Finally, by summing the equivalent control laws in Equation (26) and the reaching control laws in Equation (27), the final control laws for the underactuated subsystem are obtained as:

$$\begin{bmatrix} u_2 \\ u_3 \end{bmatrix} = \begin{bmatrix} u_{eq}^{\phi} + u_r^{\phi} \\ u_{eq}^{\theta} + u_r^{\theta} \end{bmatrix} \tag{29}$$

Theorem 2: Considering the underactuated subsystem defined in Equation (7), along with the control laws designed in Equation (29) and the adaptive laws presented in Equation (28), it is guaranteed that the tracking errors of the underactuated subsystem, as defined in Equation (21), converge to the origin in finite time and remain within a neighborhood of it.

Proof. 2: To demonstrate Theorem 2, the direct approach of Lyapunov stability analysis is utilized. Hence, the following candidate Lyapunov function is proposed:

$$V_\phi = \frac{1}{2} s_\phi^2 + \frac{1}{2\mu_1^{\phi}} \left(\tilde{K}_1^{\phi}\right)^2 + \frac{1}{2\mu_2^{\phi}} \left(\tilde{K}_2^{\phi}\right)^2 \tag{30}$$

Where the terms $\tilde{K}_1^{\phi} = \hat{K}_1^{\phi} - K_1^{\phi}$ and $\tilde{K}_2^{\phi} = \hat{K}_2^{\phi} - K_2^{\phi}$ represent the estimation errors associated with the adaptive laws in Equation (28). By differentiating the Lyapunov candidate function, we obtain:

$$\begin{aligned} \dot{V_\phi} &= s_\phi \dot{s_\phi} + \frac{1}{\mu_1^{\phi}} \tilde{K}_1^{\phi} \dot{\tilde{K}}_1^{\phi} + \frac{1}{\mu_2^{\phi}} \tilde{K}_2^{\phi} \dot{\tilde{K}}_2^{\phi} \\ &= s_\phi \left[\dot{\sigma_\phi} + \beta_\phi \left(|\sigma_\phi|^{\lambda_\phi} sgn(\sigma_\phi) + \alpha_\phi \sigma_\phi\right)\right] + \\ &\quad \frac{1}{\mu_1^{\phi}} \tilde{K}_1^{\phi} \dot{\tilde{K}}_1^{\phi} + \frac{1}{\mu_2^{\phi}} \tilde{K}_2^{\phi} \dot{\tilde{K}}_2^{\phi} \\ &= s_\phi \left[-\hat{K}_1^{\phi} sgn^{\eta_{1,\phi}}(s_\phi) - \hat{K}_2^{\phi} sgn^{\eta_{2,\phi}}(s_\phi)\right] + \\ &\quad \frac{\tilde{K}_1^{\phi}}{\mu_1^{\phi}} \left(\mu_1^{\phi} |s_\phi|\right)^{n_{1,\phi}+1} + \frac{\tilde{K}_2^{\phi}}{\mu_2^{\phi}} \left(\mu_2^{\phi} |s_\phi|\right)^{n_{2,\phi}+1} \\ &= -\hat{K}_1^{\phi} |s_\phi|^{n_{1,\phi}+1} + \hat{K}_2^{\phi} |s_\phi|^{n_{2,\phi}+1} 0 + \\ &\quad K_1^{\phi} |s_\phi|^{n_{1,\phi}+1} + K_2^{\phi} |s_\phi|^{n_{2,\phi}+1} + \\ &\quad K_1^{\phi} |s_\phi|^{n_{1,\phi}+1} - K_1^{\phi} |s_\phi|^{n_{1,\phi}+1} + \\ &\quad K_2^{\phi} |s_\phi|^{n_{2,\phi}+1} - K_2^{\phi} |s_\phi|^{n_{2,\phi}+1} \\ &= -\tilde{K}_1^{\phi} |s_\phi|^{n_{1,\phi}+1} - \tilde{K}_2^{\phi} |s_\phi|^{n_{2,\phi}+1} + \\ &\quad \tilde{K}_1^{\phi} |s_\phi|^{n_{1,\phi}+1} + \tilde{K}_2^{\phi} |s_\phi|^{n_{2,\phi}+1} - \\ &\quad K_1^{\phi} |s_\phi|^{n_{1,\phi}+1} - K_2^{\phi} |s_\phi|^{n_{2,\phi}+1} \\ &\leq -K_1^{\phi} |s_\phi|^{n_{1,\phi}+1} - K_2^{\phi} |s_\phi|^{n_{2,\phi}+1} \end{aligned} \tag{31}$$

After performing some mathematical manipulations, the subsequent expression can be formulated:

$$\begin{aligned} \dot{V_\phi} &\leq -K_1^{\phi} \left|\frac{2s_\phi^2}{2}\right|^{\frac{n_{1,\phi}+1}{2}} - K_2^{\phi} \left|\frac{2s_\phi^2}{2}\right|^{\frac{n_{2,\phi}+1}{2}} \\ \dot{V_\phi} &\leq -2K_1^{\phi} |V_\phi|^{\frac{n_{1,\phi}+1}{2}} - 2K_2^{\phi} |V_\phi|^{\frac{n_{2,\phi}+1}{2}} \end{aligned} \tag{32}$$

According to Lemma 2 in reference [9], the terms e_ϕ, e_y converges to the origin in T_{f_2}, given by:

$$T_{f_2} = \frac{1}{2K_1^{\phi}(n_{1,\phi}-1)} + \frac{1}{2K_2^{\phi}(1-n_{2,\phi})} \tag{33}$$

Following the procedure applied in Proof 2, one can also verify that the errors e_θ, e_x vanishes in finite time T_{f_3}.

4. Results and Discussions

Here, the capability of the proposed control approach is verified for the trajectory tracking task of an underactuated quad-rotor. The validation process relies on numerical simulations conducted in MATLAB/Simulink and the ROS/Gazebo platform. The simulations were conducted using the Parrot Mambo quad-rotor model, whose physical parameters are as follows: mass $m_q = 1kg$, gravitational acceleration $g = 9.81m/s^2$, moments of inertia $J_x = J_y = 0.018125kg \cdot m^2, J_z = 0.035kg \cdot m^2$, and $J_r = 2.8385 \times 10^{-5}kg \cdot m^2$. Additionally, linear friction coefficients are $k_x = k_y = k_z = 0.01N \cdot s/m$, and rotational friction coefficients are $k_\phi = k_\theta = k_\psi = 0.012N \cdot s/rad$.

The parameters of the proposed flight scheme are: $k_{d_x} = 20m_q/u_1 cos(\phi)cos(\psi), k_{p_x} = 15m_q/u_1 cos(\phi)cos(\psi), k_{i_x} = 0.0025, k_{d_y} = -20m_q/u_1 cos(\psi), k_{p_y} = -15m_q/u_1 cos(\psi), k_{i_y} = 0.0005, k_{d_\theta} = 0.01, k_{p_\theta} = 2, k_{i_\theta} = 0.025, k_{d_\phi} = 0.08, k_{p_\phi} = 2, k_{i_\phi} = 0.025, k_{d_z} = 1, k_{p_z} = 2, k_{i_z} = 0.0003, k_{d_\psi} = 1, k_{p_\psi} = 2, k_{i_\psi} = 0.0003, \mu_1^{\phi} = \mu_2^{\phi} = \mu_1^{\theta} = \mu_2^{\theta} = 5, \mu_1^{z} = \mu_2^{z} = \mu_1^{\psi} =$

$\mu_2^{\psi} = 2, \alpha_z = 1.5, \alpha_{\psi} = 1.2, \alpha_{\phi} = \alpha_{\theta} = 1.2, \beta_z = \beta_{\psi} = \beta_{\phi} = \beta_{\theta} = 2, \eta_{1,z} = \eta_{1,\psi} = \eta_{1,\phi} = \eta_{1,\theta} = 1/3, \eta_{2,z} = \eta_{2,\psi} = \eta_{2,\phi} = \eta_{2,\theta} = 1/5.$

4.1. MATLAB/Simulink

Here, the designed control methodology is implemented in the MATLAB/Simulink platform to analyze its effectiveness with respect to robustness and speed of convergence. The simulation considers a realistic flight environment affected by severe perturbations and model uncertainties. To validate the theoretical results obtained, a comparative analysis is performed between the designed control strategy and three previously reported methods in the literature: Adaptive Sliding Mode Control with Adaptive Sliding Mode Control (NN-ASMC) [24], Enhanced Dual Sliding Mode Control (UDSMC) [25], and Global Fast Terminal Sliding Mode Control (GFTSMC) [27]. The initial conditions of the four-rotor aerial system are set as $[x_0, y_0, z_0] = [1,1,0]^T$, and the reference trajectory is defined as $[x_d, y_d, z_d]^T = [2.5cos(0.2t), 2.5sin(0.2t), 2 + 0.1t]^T$ m. The desired Euler angles, corresponding to ϕ_d, θ_d, and ψ_d, are kept constant at zero throughout the experiment. The external disturbances applied are defined as:

$$\begin{aligned} d_x(t) &= -1.6sin(0.1t) + 0.8sin(0.44t) + \\ &\quad 0.16sin(1.75t) + 0.112sin(0.28t)[m/s^2] \\ d_y(t) &= sin(0.4t) + cos(0.7t)[m/s^2] \\ d_z(t) &= 0.8cos(0.7t)[m/s^2] \\ d_{\phi}(t) &= d_{\theta}(t) = d_{\psi}(t) = 0.2cos(0.7t)[rad/s^2] \end{aligned} \quad (34)$$

Parametric uncertainties represent variations in the physical parameters of the four-rotor robot. In this research, a +30% variation is considered in both the mass and the moments of inertia, i.e., $m_q = 1.3, J_x = J_y = 0.0236\ kg \cdot m^2, J_z = 0.0455\ kg \cdot m^2$. The results of the simulations are presented in Figures 3-9. The quad-rotor's 3D and 2D flight trajectories under different control strategies are illustrated in Figures 3 and 4.

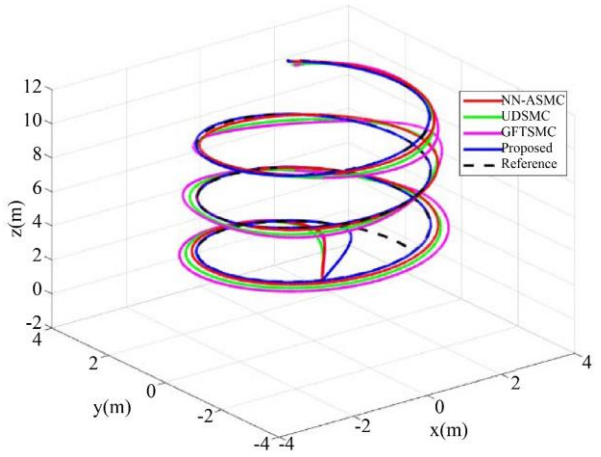

Fig. 3 3D trajectory tracking under different control strategies

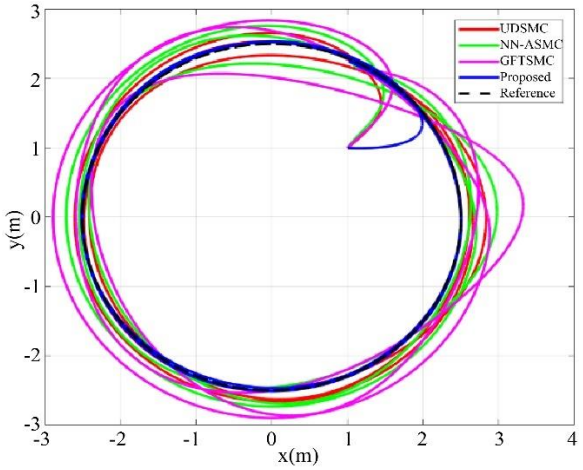

Fig. 4 2D trajectory projections of the quad-rotor

A preliminary analysis reveals that the proposed control exhibits greater robustness in trajectory tracking under large perturbations and uncertainties of modelling, in comparison with the UDSMC, NN-ASMC, and GFTSMC strategies. The Cartesian position and linear velocity trajectories are illustrated in Figures 5 and 6.A closer inspection of these curves, particularly the zoomed-in portions of Figure 5, reveals that the developed control scheme provides enhanced robustness and accelerated convergence when subjected to external perturbations, outperforming the benchmark strategies.

The errors are depicted in Figure 7 to support these findings further. This figure shows that the designed controller attains quicker finite-time convergence to the origin while remaining bounded within a small neighborhood throughout the entire flight mission, despite disturbances and dynamic uncertainties. In contrast, the UDSMC, NN-ASMC, and GFTSMC strategies exhibit notable fluctuations and deviations in the tracking errors, with GFTSMC being the most affected.

Collectively, Figures 5, 6, and 7 highlight the enhanced performance of the suggested scheme in terms of robustness and finite-time convergence. This enhanced performance is attributed to the advanced design based on recursive sliding mode control, along with the implementation of robust adaptive laws. Figure 8 illustrates the Euler angles-roll, pitch, and yaw-of the aerial robot, while the control signals generated by each strategy are presented in Figure 9.

From this latter figure, it can be observed that the control signals of the suggested controller are smoother and show a significant reduction in chattering, even under strong external disturbances. In an attempt to derive a detailed numerical assessment of the controllers' performance regarding robustness and convergence speed, two indicators were considered: RMSE and the settling time. The resulting values for each strategy are reported in Tables 1 and 2.

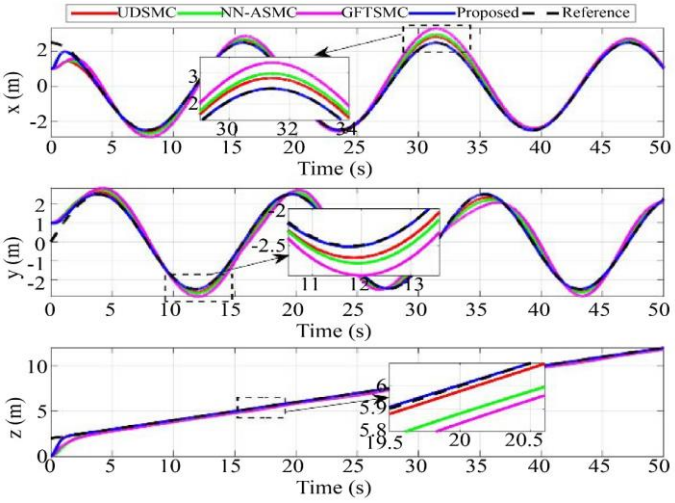

Fig. 5 Cartesian position responses

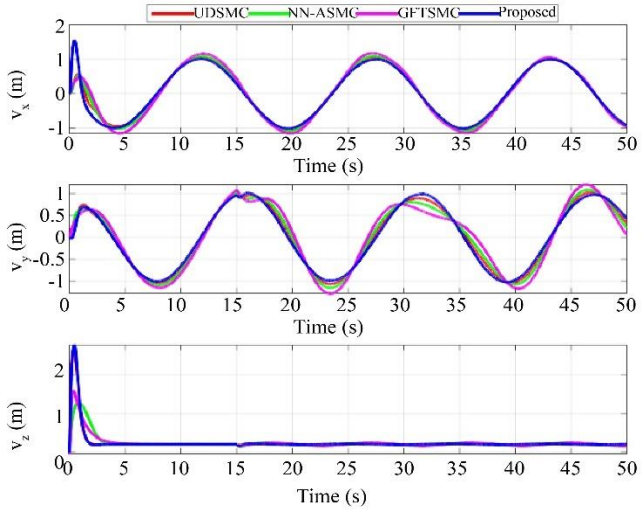

Fig. 6 Linear velocity responses

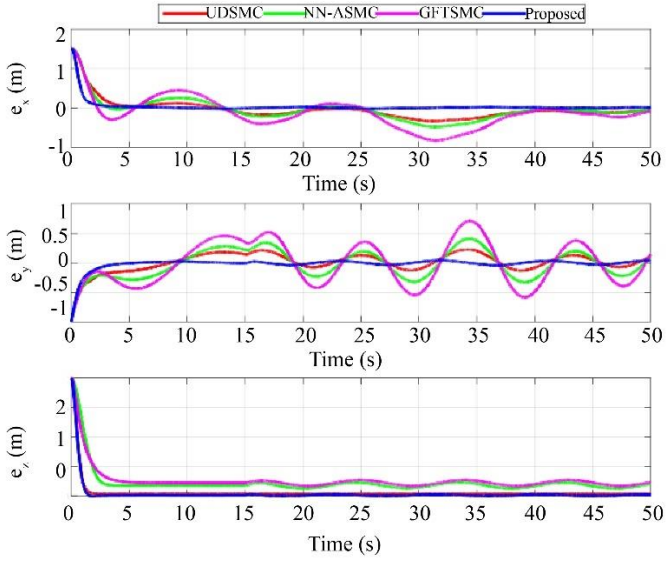

Fig. 7 Position tracking errors

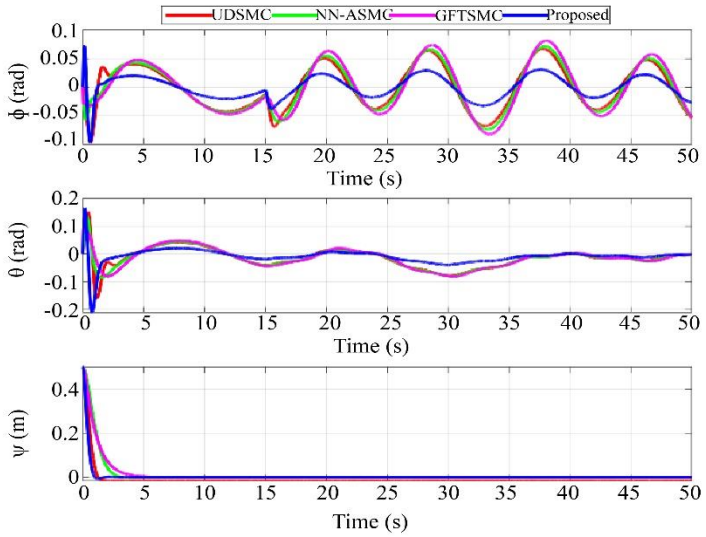

Fig. 8 Euler angle responses

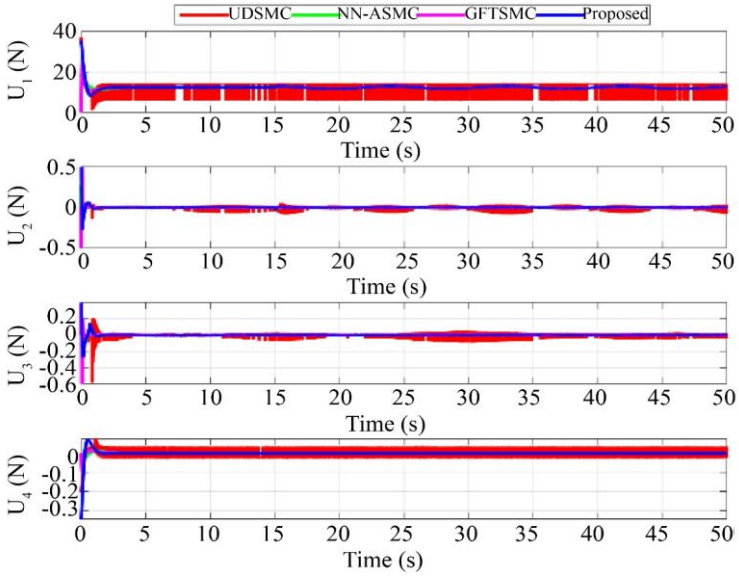

Fig. 9 Control input signals generated by each control strategy

Table 1. RMSE of position tracking

Control strategy	RMSE		
	x	*y*	*z*
NN-ASMC	0.272	0.220	0.261
UDSMC	0.226	0.139	0.098
GFTSMC	0.418	0.356	0.276
Proposed	0.088	0.064	0.098

Table 2. Settling time of position tracking errors

Control strategy	Settling time		
	x	*y*	*z*
NN-ASMC	4.249	4.597	3.298
UDSMC	5.069	4.944	3.210
GFTSMC	3.440	3.698	4.120
Proposed	2.612	2.830	2.169

According to the values reported in Table 1, the proposed control strategy yields the lowest RMSE values across all tracking errors, indicating more accurate trajectory tracking. Conversely, the GFTSMC strategy exhibits the highest RMSE values, making it the most affected by disturbances. Meanwhile, Table 2 shows that the proposed approach achieves the shortest convergence times in position tracking errors along all three axes, indicating a faster finite-time response toward the reference signal when compared to the UDSMC, NN-ASMC, and GFTSMC controllers.

4.2. ROS / Gazebo

After the simulation study in Matlab/Simulink, in this section, the focus is on executing the ROS/Gazebo-based Software-In-The-Loop (SITL) simulation to evaluate the proposed control strategy in a highly realistic environment.

Performing these simulations in ROS/Gazebo is essential before conducting practical outdoor flight experiments. From a pragmatic point of view, the experiments at SITL excel in their ability to faithfully recreate real-world conditions, surpassing the proof of concept conducted in MATLAB/Simulink. In this context, the controller is implemented in ROS using the C++ programming language. Subsequently, the integration of the control node with the 3DR Iris quadcopter model is carried out, and the behavior of the quadcopter is visualized in the Gazebo simulator. Figure 10 shows the 3DR Iris quadcopter in the Gazebo simulation environment.

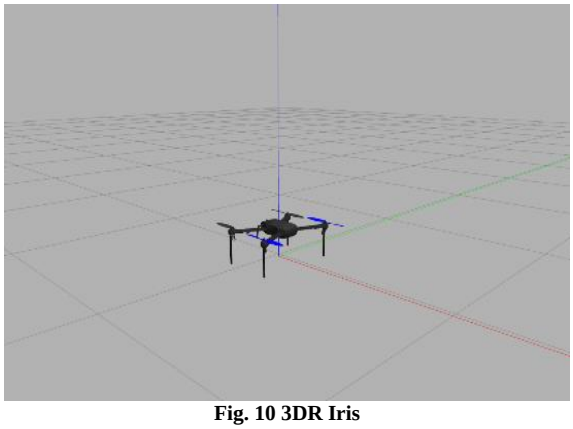

Fig. 10 3DR Iris

To evaluate the capabilities of the suggested approach in a pseudo-real scenario, a comparative study with the built-in PID controller and the second-order SMC is performed. The desired trajectory is set as $[x_d, y_d, z_d]^T = [5sin(0.2t), 5cos(0.2t), 3]^T$m.

The results obtained using ROS/Gazebo are illustrated in Figures 11-15. Figure 11 depicts the trajectory of the quad-rotor aerial robot in 3D with the different controllers, whereas Figure 12 visualizes this in 2D. On the other hand, the temporal evolution of the quad-rotor position is exhibited in Figure 13. In this analysis, it is observed that our proposed approach achieves significant enhancements in both convergence rate and tracking precision when compared with conventional PID and standard SMC controllers. The PID controller, as a classical linear scheme, initially exhibits oscillations, especially in the x and y axes, before stabilization in time. Although the SMC does not exhibit oscillations, it has a slower response to converge to the desired trajectory due to its asymptotic stability. In contrast, our proposed control strategy stands out for its ability to converge rapidly in a finite time to the desired trajectory. This feature is reflected in Figure 14, where the tracking errors of the proposed controller converge rapidly to zero and remain consistently in the neighborhood of the origin. Finally, Figure 15 presents the response of the quad-rotor attitude, thus completing the performance analysis of the control system.

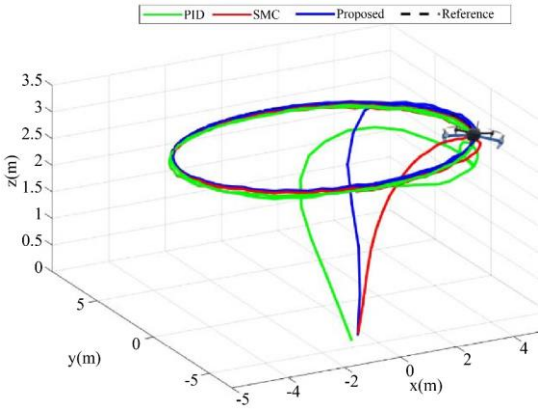

Fig. 11 3D trajectory of the four-rotor UAV

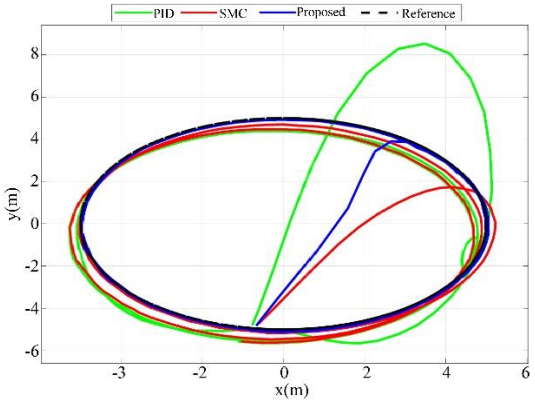

Fig. 12 2D trajectory of the four-rotor UAV

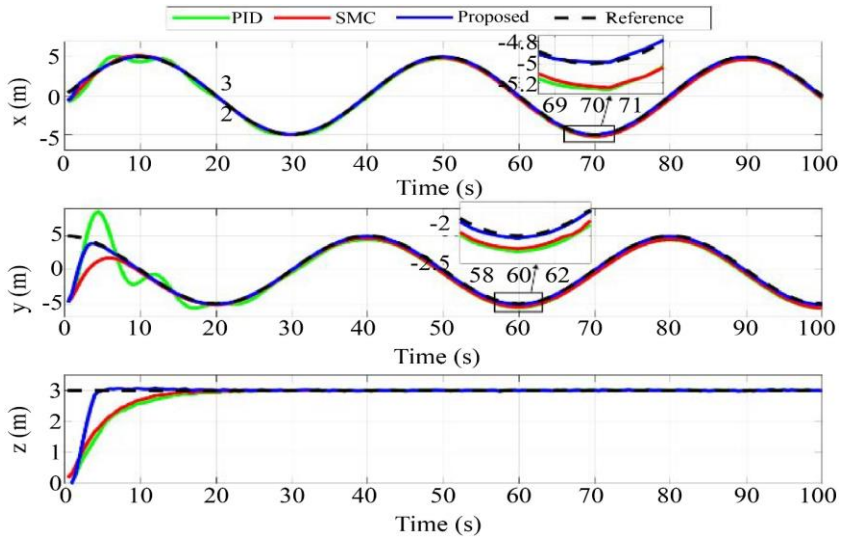

Fig. 13 Temporal position response

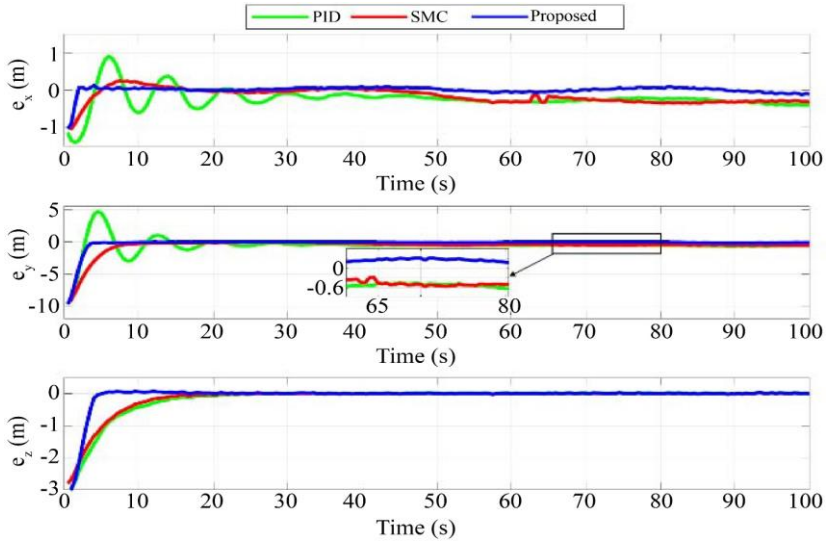

Fig. 14 Position tracking errors

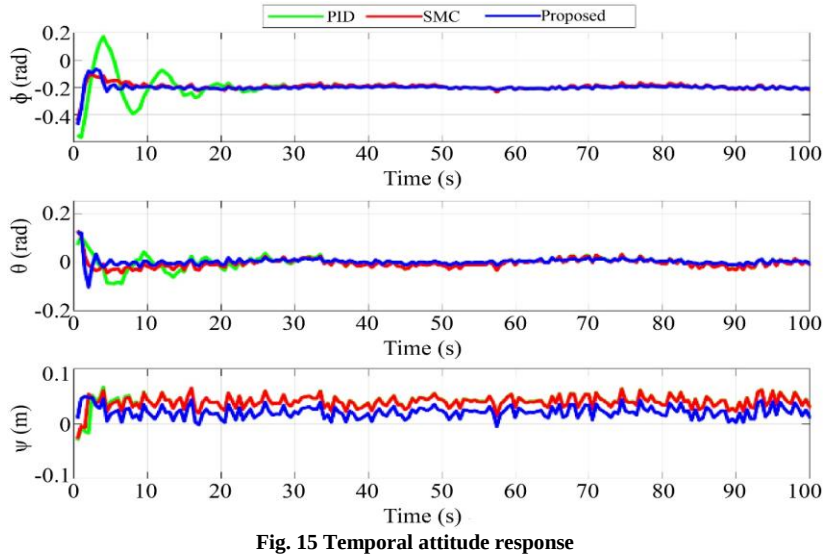

Fig. 15 Temporal attitude response

5. Conclusion

In the present work, a novel finite-time robust adaptive control methodology has been proposed to tackle the trajectory tracking task of an underactuated quad-rotor in the presence of perturbations and uncertainties in the modeling. The developed method respects the underactuated structure of the quad-rotor system and is based on recursive sliding mode control theory, combining a PID-type sliding surface with a fast terminal integral sliding surface, along with robust adaptive laws. This control architecture enhances the system's tracking accuracy, convergence speed, and robustness. Simulation results, supported by a quantitative evaluation using metrics such as RMSE and settling time, have demonstrated that the proposed control approach outperforms the NN-ASMC, UDSMC, and GFTSMC strategies in terms of fast convergence and robustness against perturbations and uncertainties. As future work, this strategy will be extended to distributed formation control of multiple underactuated quad-rotors and cooperative control for suspended load transportation. Additionally, the experimental deployment of the proposed controller is planned for future investigations.

Acknowledgments

The authors would like to express their gratitude to the National University of San Agustin of Arequipa, Peru. Author 1 (Cristhian Mirko Ccorimanya Alvarez), Author 2 (Edson Dario Ccolla Pariapaza), and Author 3 (Lizardo Pari) contributed equally to this work.

References

[1] Moad Idrissi, Mohammad Salami, and Fawaz Annaz, "A review of Quadrotor Unmanned Aerial Vehicles: Applications, Architectural Design and Control Algorithms," *Journal of Intelligent & Robotic Systems*, vol. 104, no. 2, pp. 1-33, 2022. [CrossRef] [Google Scholar] [Publisher Link]

[2] Robert Mahony, Vijay Kumar, and Peter Corke, "Multirotor Aerial Vehicles: Modeling, Estimation, and Control of Quadrotor," *IEEE Robotics & Automation Magazine*, vol. 19, no. 3, pp. 20-32, 2012. [CrossRef] [Google Scholar] [Publisher Link]

[3] Bara J. Emran, and Homayoun Najjaran, "A Review of Quadrotor: An Underactuated Mechanical System," *Annual Reviews in Control*, vol. 46, pp. 165-180, 2018. [CrossRef] [Google Scholar] [Publisher Link]

[4] Luis F. Canaza Ccari, and Pablo Raul Yanyachi, "A Novel Neural Network-Based Robust Adaptive Formation Control for Cooperative Transport of a Payload using Two Underactuated Quadcopters," *IEEE Access*, vol. 11, pp. 36015-36028, 2023. [CrossRef] [Google Scholar] [Publisher Link]

[5] Ivan Lopez-Sanchez, and Javier Moreno-Valenzuela, "PID Control of Quadrotor UAVs: A Survey," *Annual Reviews in Control*, vol. 56, 2023. [CrossRef] [Google Scholar] [Publisher Link]

[6] Changlong Liu, Jian Pan, and Yufang Chang, "PID and LQR Trajectory Tracking Control for an Unmanned Quadrotor Helicopter: Experimental Studies," *2016 35th Chinese Control Conference (CCC)*, Chengdu, China, pp. 10845-10850, 2016. [CrossRef] [Google Scholar] [Publisher Link]

[7] Necdet Sinan Özbek Nozbek, Mert Önkol, and Mehmet Önder Ef, "Feedback Control Strategies for Quadrotor-Type Aerial Robots: A Survey," *Transactions of the Institute of Measurement and Control*, vol. 38, no. 5, pp. 529-554, 2016. [CrossRef] [Google Scholar] [Publisher Link]

[8] Marco Rinaldi, Stefano Primatesta, and Giorgio Guglieri, "A Comparative Study for Control of Quadrotor UAVs," *Applied Sciences*, vol. 13, no. 6, pp. 1-20, 2023. [CrossRef] [Google Scholar] [Publisher Link]

[9] Omar Mechali et al., "Observer-Based Fixed-Time Continuous Nonsingular Terminal Sliding Mode Control of Quadrotor Aircraft Under Uncertainties and Disturbances for Robust Trajectory Tracking: Theory and Experiment," *Control Engineering Practice*, vol. 111, 2021. [CrossRef] [Google Scholar] [Publisher Link]

[10] Luis F. Canaza Ccari et al., "Robust Finite-Time Adaptive Nonlinear Control System for an EOD Robotic Manipulator: Design, Implementation and Experimental Validation," *IEEE Access*, vol. 12, pp. 93859-93875, 2024. [CrossRef] [Google Scholar] [Publisher Link]

[11] Yuri Shtessel et al., *Sliding Mode Control and Observation*, 1st ed., Springer, Birkhäuser New York, 2014. [CrossRef] [Google Scholar] [Publisher Link]

[12] Ahmad Taher Azar, and Quanmin Zhu, *Advances and Applications in Sliding Mode Control Systems*, 1st ed., Springer Cham, 2015. [CrossRef] [Google Scholar] [Publisher Link]

[13] Shafiqul Islam, and Xiaoping P. Liu, "Robust Sliding Mode Control for Robot Manipulators," *IEEE Transactions on Industrial Electronics*, vol. 58, no. 6, pp. 2444-2453, 2010. [CrossRef] [Google Scholar] [Publisher Link]

[14] Jian Xu, Man Wang, and Lei Qiao, "Dynamical Sliding Mode Control for the Trajectory Tracking of Underactuated Unmanned Underwater Vehicles," *Ocean Engineering*, vol. 105, pp. 54-63, 2015. [CrossRef] [Google Scholar] [Publisher Link]

[15] Xingyang Lu et al., "Neural Network Adaptive Sliding Mode Control for Omnidirectional Vehicle with Uncertainties," *ISA Transactions*, vol. 86, pp. 201-214, 2019. [CrossRef] [Google Scholar] [Publisher Link]

[16] Héctor Ríos et al., "Continuous Sliding-Mode Control Strategies for Quadrotor Robust Tracking: Real-Time Application," *IEEE Transactions on Industrial Electronics*, vol. 66, no. 2, pp. 1264-1272, 2018. [CrossRef] [Google Scholar] [Publisher Link]

[17] Lulu Chen et al., "Robust Adaptive Recursive Sliding Mode Attitude Control for a Quadrotor with Unknown Disturbances," *ISA Transactions*, vol. 122, pp. 114-125, 2022. [CrossRef] [Google Scholar] [Publisher Link]

[18] Jun Zhou et al., "Active Finite-Time Disturbance Rejection Control for Attitude Tracking of Quad-Rotor Under Input Saturation," *Quad-Rotor Under Input Saturation*, vol. 357, no. 16, pp. 11153-11170, 2020. [CrossRef] [Google Scholar] [Publisher Link]

[19] Omid Mofid, Saleh Mobayen, and Afef Fekih, "Adaptive Integral-Type Terminal Sliding Mode Control for Unmanned Aerial Vehicle Under Model Uncertainties and External Disturbances," *IEEE Access*, vol. 9, pp. 53255-53265, 2021. [CrossRef] [Google Scholar] [Publisher Link]

[20] Ning Wang et al., "Hybrid Finite-Time Trajectory Tracking Control of a Quadrotor," *ISA Transactions*, vol. 90, pp. 278-286, 2019. [CrossRef] [Google Scholar] [Publisher Link]

[21] Moussa Labbadi et al., "Fractional-Order Global Sliding Mode Controller for an Uncertain Quadrotor UAVs Subjected to External Disturbances," *Journal of the Franklin Institute*, vol. 358, pp. 4822-4847, 2021. [CrossRef] [Google Scholar] [Publisher Link]

[22] Rong Xu, and Umit Ozguner, "Sliding Mode Control of a Quadrotor Helicopter," *Proceedings of the 45th IEEE Conference on Decision and Control*, San Diego, CA, USA, pp. 4957-4962, 2006. [CrossRef] [Google Scholar] [Publisher Link]

[23] En-Hui Zheng, Jing-Jing Xiong, and Ji-Liang Luo, "Second Order Sliding Mode Control for a Quadrotor UAV," *ISA Transactions*, vol. 53, pp. 1350-1356, 2014. [CrossRef] [Google Scholar] [Publisher Link]

[24] Hadi Razmi, and Sima Afshinfar, "Neural Network-Based Adaptive Sliding Mode Control Design for Position and Attitude Control of a Quadrotor UAV," *Aerospace Science and Technology*, vol. 91, pp. 12-27, 2019. [CrossRef] [Google Scholar] [Publisher Link]

[25] Ruobing Li et al., "Trajectory Tracking of a Quadrotor using Extend State Observer based U-Model Enhanced Double Sliding Mode Control," *Journal of the Franklin Institute*, vol. 360, no. 4, pp. 3520-3544, 2023. [CrossRef] [Google Scholar] [Publisher Link]

[26] Luis F. Canaza Ccari et al., "Distributed Robust Adaptive Control for Finite-Time Flight Formation of Multi-Quadcopter Systems with Large Lumped Uncertainties," *IEEE Access*, vol. 12, pp. 113384-113405, 2024. [CrossRef] [Google Scholar] [Publisher Link]

[27] Jing-Jing Xiong, and Guo-Bao Zhang, "Global Fast Dynamic Terminal Sliding Mode Control for a Quadrotor UAV," *ISA Transactions*, vol. 66, pp. 233-240, 2017. [CrossRef] [Google Scholar] [Publisher Link]

[28] Aminurrashid Noordin, Mohd Ariffanan Mohd Basri, and Zaharuddin Mohamed, "Real-Time Implementation of an Adaptive PID Controller for the Quadrotor MAV Embedded Flight Control System," *Aerospace*, vol. 10, no. 1, pp. 1-24, 2023. [CrossRef] [Google Scholar] [Publisher Link]